National Library of Canada
Acquisitions and Bibliographic Services Branch
395 Wellington Street
Ottawa, Ontario
K1A 0N4

Bibliothèque nationale du Canada
Direction des acquisitions et des services bibliographiques
395, rue Wellington
Ottawa (Ontario)
K1A 0N4

Your file Votre référence

Our file Notre référence

NOTICE

The quality of this microform is heavily dependent upon the quality of the original thesis submitted for microfilming. Every effort has been made to ensure the highest quality of reproduction possible.

If pages are missing, contact the university which granted the degree.

Some pages may have indistinct print especially if the original pages were typed with a poor typewriter ribbon or if the university sent us an inferior photocopy.

Reproduction in full or in part of this microform is governed by the Canadian Copyright Act, R.S.C. 1970, c. C-30, and subsequent amendments.

AVIS

La qualité de cette microforme dépend grandement de la qualité de la thèse soumise au microfilmage. Nous avons tout fait pour assurer une qualité supérieure de reproduction.

S'il manque des pages, veuillez communiquer avec l'université qui a conféré le grade.

La qualité d'impression de certaines pages peut laisser à désirer, surtout si les pages originales ont été dactylographiées à l'aide d'un ruban usé ou si l'université nous a fait parvenir une photocopie de qualité inférieure.

La reproduction, même partielle, de cette microforme est soumise à la Loi canadienne sur le droit d'auteur, SRC 1970, c. C-30, et ses amendements subséquents.

Canada

UNIVERSITY OF ALBERTA

LINEAR STABILITY OF ROTATING BOUNDARY LAYERS

BY

ROBERT MICHAEL PROKOP

©

A THESIS SUBMITTED TO THE FACULTY OF GRADUATE STUDIES AND RESEARCH IN PARTIAL FULFILMENT OF THE REQUIREMENTS FOR THE DEGREE OF MASTER OF SCIENCE.

DEPARTMENT OF MECHANICAL ENGINEERING

EDMONTON, ALBERTA

FALL, 1993

National Library of Canada
Acquisitions and Bibliographic Services Branch
395 Wellington Street
Ottawa, Ontario
K1A 0N4

Bibliothèque nationale du Canada
Direction des acquisitions et des services bibliographiques
395, rue Wellington
Ottawa (Ontario)
K1A 0N4

Your file - Votre référence

Our file - Notre référence

The author has granted an irrevocable non-exclusive licence allowing the National Library of Canada to reproduce, loan, distribute or sell copies of his/her thesis by any means and in any form or format, making this thesis available to interested persons.

L'auteur a accordé une licence irrévocable et non exclusive permettant à la Bibliothèque nationale du Canada de reproduire, prêter, distribuer ou vendre des copies de sa thèse de quelque manière et sous quelque forme que ce soit pour mettre des exemplaires de cette thèse à la disposition des personnes intéressées.

The author retains ownership of the copyright in his/her thesis. Neither the thesis nor substantial extracts from it may be printed or otherwise reproduced without his/her permission.

L'auteur conserve la propriété du droit d'auteur qui protège sa thèse. Ni la thèse ni des extraits substantiels de celle-ci ne doivent être imprimés ou autrement reproduits sans son autorisation.

ISBN 0-315-88031-7

Canada

UNIVERSITY OF ALBERTA

RELEASE FORM

NAME OF AUTHOR: Robert Michael Prokop

TITLE OF THESIS: Linear Stability of Rotating Boundary Layers

DEGREE: Master of Science

YEAR THIS DEGREE GRANTED: 1993

PERMISSION IS HEREBY GRANTED TO THE UNIVERSITY OF ALBERTA LIBRARY TO REPRODUCE SINGLE COPIES OF THIS THESIS AND TO LEND OR SELL SUCH COPIES FOR PRIVATE, SCHOLARLY, OR SCIENTIFIC RESEARCH PURPOSES ONLY.

THE AUTHOR RESERVES ALL OTHER PUBLICATION AND OTHER RIGHTS IN ASSOCIATION WITH THE COPYRIGHT IN THE THESIS, AND EXCEPT AS HEREINBEFORE PROVIDED, NEITHER THE THESIS NOR ANY SUBSTANTIAL PORTION THEREOF MAY BE PRINTED OR OTHERWISE REPRODUCED IN ANY MATERIAL FORM WHATEVER WITHOUT THE AUTHOR'S PRIOR WRITTEN PERMISSION.

Rob Prokop

422-52313 Range Road 232
Sherwood Park, AB
T8B 1B7

Date: Sept 14/93

UNIVERSITY OF ALBERTA

FACULTY OF GRADUATE STUDIES AND RESEARCH

THE UNDERSIGNED CERTIFY THAT THEY HAVE READ, AND RECOMMEND TO THE FACULTY OF GRADUATE STUDIES AND RESEARCH FOR ACCEPTANCE, A THESIS ENTITLED *LINEAR STABILITY OF ROTATING BOUNDARY LAYERS* SUBMITTED BY ROBERT MICHAEL PROKOP IN PARTIAL FULFILMENT OF THE REQUIREMENTS FOR THE DEGREE OF MASTER OF SCIENCE.

W. Finlay

Dr. W. H. Finlay

K.C. Cheng

Dr. K. C. Cheng

K Nandakumar

Dr. K. Nandakumar

Date: Sept 14/93

ABSTRACT

In this study, the linear stability of flow over a rotating flat plate which leads to Görtler-type vortices is examined. The parabolized governing equations are solved using a Legendre spectral element method with a marching scheme. The normal component of the Coriolis force is dominant and causes the development of the boundary layer to be suppressed. For sufficiently low rotation rates, the suppression of the boundary layer thickness is negligible and a rotational Görtler number is the appropriate parameter to describe the growth of the vortices. At higher rotation rates, it is no longer possible to apply the rotational Görtler number; the most unstable wavelength is dependent on both the rotation number Ro_x and the Reynolds number Re_x. Although unique neutral stability curves do not exist, the results agree quite well with previous local stability analysis when sufficiently far from the leading edge.

ACKNOWLEDGEMENTS

I wish to thank my supervisor, Dr. W. H. Finlay, for his words of advice and Dr. Y. Guo for his assistance with the computer code during the early stages of the study.

I would also like to thank my parents for their support. Thanks are also due to the graduate students in the Department of Mechanical Engineering for providing an enjoyable atmosphere in which to work.

Financial support for this project was provided by the Natural Science and Engineering Research Council of Canada.

TABLE OF CONTENTS

1.0 INTRODUCTION 1

2.0 LINEAR STABILITY OF ROTATING BOUNDARY LAYERS 3

2.1 Background Information 3

2.2 Theory and Numerical Methods 4

2.3 Base Flow 6

2.4 Linear Stability of the Base Flow 9

2.4.1 Linear Stability for Low Rotation Rates 11

2.4.2 Linear Stability for Moderate and High Rotation Rates . 13

2.4.3 Comparison to Local Stability Analysis 14

Chapter 2 References 23

3.0 CONCLUSION 25

3.1 Summary 25

3.2 Future Work 26

Chapter 3 References 28

APPENDIX: Description of the Numerical Method 29

LIST OF FIGURES

Figure 2.1. The geometry and sign convention of flow over a rotating flat plate is shown. Only a small section away from the leading edge is illustrated 16

Figure 2.2. The variation in boundary layer thickness δ with rotation rate is compared to the nonrotating Blasius thickness δ_B 17

Figure 2.3. The velocity profile is shown for low rotation rate $Ro_x/Re_x = 2x10^{-6}$ (circles) and high rotation rate $Ro_x/Re_x = 25x10^{-5}$ (triangles) 18

Figure 2.4. Variation in growth rate with Λ_{Re} and Re_x for $Ro_x/Re_x = 1x10^{-5}$. The most unstable wavelength is indicated by the dotted line . . 19

Figure 2.5. A comparison of experimentally observed wavelengths (◯) and the linearly most unstable wavelengths calculated in this study (●) and a local stability analysis[4] (▲) 20

Figure 2.6. The variation in the linearly most unstable wavelength Λ_G of vortices with rotational Görtler number is shown. This figure is applicable to low rates of rotation ($Ro_x/Re_x \leq 10^{-5}$) 21

Figure 2.7. The linearly most unstable wavelength Λ_{Re} is shown as a function of Ro_x and Re_x 22

SYMBOLS AND NOMENCLATURE

Roman Symbols

G	Görtler number for flow over a concave plate
G_{rot}	Görtler number for flow over a rotating flat plate
p	pressure
p^*	sum of pressure gradient and centrifugal force
R	position vector
Re_x	Reynolds number
Ro_x	rotation number
u_i	i-th component of velocity
$\tilde{u}$	complex eigenfunction for the perturbation
U_∞	free stream velocity
x	streamwise distance
x_i	i-th component of distance
X	downstream distance from the leading edge of the plate
X_o	downstream distance where the initial condition is supplied
y	normal distance
z	spanwise distance

Greek Symbols

∂	partial derivative
β	perturbation wavenumber

δ	boundary layer thickness
Ω	rotation rate of the plate
λ	dimensional wavelength of the vortices
Λ	nondimensional wavelength of the vortices
ν	kinematic viscosity of the fluid
ρ	density of the fluid
τ	time

CHAPTER 1

1.0 INTRODUCTION[1]

The flow over a flat plate rotating about a spanwise axis is a simple geometry in which streamwise-oriented vortices are induced. Like the Görtler problem (flow over a concave plate), the mechanism for the transition to turbulence begins with the growth of these vortices. Although the Görtler problem has been well-studied, there is little previous research on the stability of rotating boundary layers. The study of the flow over a rotating flat plate is the simplest possible rotating boundary layer. Through the analysis of this geometry, insight can be gained into the transition to turbulence for more complex rotating boundary layers such as the flow over pump impellers and turbine blades.

Though an analogy can be made between a rotating boundary layer and the Görtler problem, there are several differences between the two geometries. The Görtler problem is restricted to a large radius of curvature to simplify the governing equations and to avoid separation of the boundary layer. However, there is no analogous restriction in the amount of rotation for a rotating boundary layer. In the Görtler problem, the vortices are the result of the normal component

[1] A version of this chapter has been submitted for publication. Prokop & Finlay 1993. Physics of Fluids A.

of the centrifugal force. For a rotating boundary layer, the normal component of the Coriolis force causes the instability.

The study of the stability of boundary layers such as the rotating flat plate and the Görtler problem is particularly interesting since there is no critical onset of instability. The flow is unstable to spanwise perturbations at all points in the flow. In comparison, fully-developed flows such as curved channel flow (the Dean problem) and the rotating channel do have a critical onset of instability. Below the critical value of the governing parameter (e.g. the Dean number for the curved channel), the flow is stable to all spanwise perturbations. However, once this critical value is exceeded, the flow becomes unstable. The fact that the base flow is fully developed in these cases may be the reason for the critical onset of instability since the boundary layer velocity profile changes as it moves downstream.

In the present study, the effect of the Coriolis force on the development of the non-Blasius boundary layer is taken in account. This is discussed in section 2.3. In section 2.4, the linear growth of the Görtler-type vortices in the boundary layer is examined using a marching scheme and these results are compared to a previous local stability analysis.

CHAPTER 2

2.0 LINEAR STABILITY OF ROTATING BOUNDARY LAYERS[2]

2.1 Background Information

Figure 1 shows a sketch of the geometry and coordinate system considered in this study. The angular velocity of rotation of the plate Ω is perpendicular to the streamwise direction. The orientation of the vortices is also indicated in the figure. The generally accepted sign convention for this system would denote the rotation shown in Figure 2.1 as negative rotation. This direction of rotation tends to stabilize the system compared to the nonrotating case[1,2,3,4]. The flow on the other side of the plate (the side not visible in Figure 2.1) is usually called the unstable side and turbulent transition via the usual nonrotating flat plate routes is enhanced by the rotation. Since only negative rotation is considered in this study, the sign to indicate the direction of the rotation is ignored and all nondimensional quantities are positive.

To the author's knowledge, the first analysis of the stability of flow over a rotating flat plate was performed by Chawla[1], in which the local stability of the Blasius profile was considered. Subsequently, Koyama et al[2] measured the effects

[2] A version of this chapter has been submitted for publication. Prokop & Finlay 1993. Physics of Fluids A.

of Coriolis force on a two dimensional flat plate boundary layer. They found that on the stabilized side, the boundary layer remains laminar and its development is suppressed. Masuda and Matsubara[3] showed experimentally that the flow on the destabilized side is characterized by turbulent spots, while vortex structures similar to Görtler vortices appear on the stabilized side. They found that the vortex spacing on the stabilized side decreases with increasing rotation number and decreasing Reynolds number. Matsubara & Masuda[4] experimentally measured the wavelengths of the vortices on the stabilized side. They also used a temporal stability analysis to calculate the most unstable wavelengths and to produce a unique neutral stability curve.

2.2 Theory and numerical methods

The Navier-Stokes equations for the flow geometry in Figure 2.1 are as follows:

$$\frac{\partial \bar{u}_i}{\partial \bar{\tau}} + \bar{u}_j \frac{\partial \bar{u}_i}{\partial \bar{x}_j} = -\frac{1}{\rho}\frac{\partial \bar{p}^*}{\partial \bar{x}_i} + \nu \frac{\partial^2 \bar{u}_i}{\partial \bar{x}_j \partial \bar{x}_j} + 2e_{ijk}\bar{u}_j\bar{\Omega}_k \qquad (1)$$

where the bars denote dimensional quantities and p^* is the sum of the pressure gradient and the centrifugal force:

$$-\bar{p}^* = -\frac{\bar{p}}{\rho} + \left(\frac{1}{2}|\,\bar{\Omega}_k \bar{R}_l e_{ikl}\,|\right)^2 \qquad (2)$$

Here R_l is the position vector. In this study, the rotation vector has the form

$$\vec{\Omega}=(0,0,\Omega) \tag{3}$$

so that the plate rotates about its leading edge.

Introducing the following nondimensional variables, where X is the length along the plate and U_∞ is the free stream velocity,

$$x_i=\frac{\bar{x}_i}{X} \quad u_i=\frac{\bar{u}_i}{U_\infty} \quad p^*=\frac{\bar{p}^*}{\rho U_\infty^2} \tag{4}$$

and the rotation number Ro_x and the Reynolds number Re_x,

$$Ro_x=\frac{\Omega X}{U_\infty} \quad Re_x=\frac{U_\infty X}{\nu} \tag{5}$$

results in the following nondimensional equation for steady flow:

$$u_j\frac{\partial u_i}{\partial x_j}=-\frac{\partial p^*}{\partial x_i}+\frac{1}{Re_x}\frac{\partial^2 u_i}{\partial x_j \partial x_j}+2Ro_x e_{ijk}\delta_{k3}u_j \tag{6}$$

The stability equations are produced by inserting a spanwise perturbation of the form

$$u'=\tilde{u}\exp(i\beta z) \tag{7}$$

into equation (6). Here β is the perturbation wavenumber and $\tilde{u}$ is a complex eigenfunction. The complex eigenfunction varies in the normal and spanwise directions at a given streamwise location in the flow. A vector plot of the complex eigenfunction shows that it takes the form of streamwise-oriented pairs of counter-rotating vortices.

Taking the usual large Re_x limit results in a set of parabolic equations since the streamwise diffusion terms can be neglected[5]. This is due to the fact that the variation in the velocity profile varies much more slowly in the streamwise direction than in the cross stream plane. The computer code used to solve these equations and the accompanying stability equations is virtually the same as the code used to study Dean vortices and Görtler vortices by Guo & Finlay[6] and Guo[7]. In these studies, a Legendre spectral element method was used to solve the parabolized governing and stability equations with a marching technique. Consequently, since the solution is found as the streamwise location is varied, this stability analysis is of a convective nature. The Legendre spectral element method combines the high accuracy of spectral methods with the geometric flexibility of finite element methods. Thus, it was possible to study Dean vortices, Görtler vortices, and the rotating flat plate vortices with the same code by incorporating the appropriate boundary conditions. Extensive comparisons with experiments on Dean and Görtler vortices (see Guo & Finlay[6] and Guo[7]) and the nonrotating flat plate boundary layer were performed in order to validate the code. A brief discussion of the numerical scheme employed by the code may be found in the Appendix, and a more detailed description may be found in Guo[7].

2.3 Base Flow

The *base flow* refers to the two-dimensional boundary layer velocity profile in which the vortices develop. For a stationary flat plate, the base flow is a

Blasius profile. However, once the plate is subjected to rotation, there are Coriolis and centrifugal forces placed on the flow and no analytical or semi-analytical solution is available; the base flow is calculated instead. This calculated profile is then input into the stability code, where a perturbation is introduced and the parabolized stability equations are solved.

One of the difficulties in calculating the base profile is that an initial condition for the profile must be supplied at some distance X_o from the leading edge due to the singularity at the leading edge. For a given rotation rate, a scaled Blasius profile was used as the initial condition at the start of the computation. This was a reasonable choice since it satisfies the boundary conditions at the wall and at infinity. It was found that as the computation proceeded downstream, the boundary layer thickness eventually became a constant fraction of the Blasius solution. The closer the initial condition for the boundary layer thickness was to this constant value, the faster the solution converged to the constant fraction downstream. Furthermore, this value was independent of the location at which the initial condition was supplied. Therefore, this profile is believed to be the similarity boundary layer thickness of the governing equations and it was used as the boundary layer thickness at X_o.

The nondimensional rotation rate Ro_x/Re_x is the ratio of the force which suppresses the development of the boundary layer and the forces which result in its development. This ratio is constant as the flow moves downstream since it

does not contain a length scale. Consequently, it is physically reasonable that the boundary layer thickness is a constant fraction of the Blasius boundary layer thickness.

The Coriolis force on the flow increases as the rotation rate increases. The normal component of this force acts towards the plate, while the streamwise component acts in the downstream direction. Because the streamwise component of the force depends on streamwise location, its presence precludes a self-similar solution to the equations. However, at low rotation rates, the normal component dominates, and the appearance of self-similarity is possible.

The normal component of the Coriolis force not only induces the vortices to form, but causes the boundary layer to become thinner. The higher the rotation rate, the greater the normal pressure gradient and the thinner the boundary layer. This trend is shown in Figure 2.2, where δ is the point at which the streamwise velocity is 99% of the free stream value and δ_B is the boundary layer thickness of the nonrotating case (i.e., the Blasius boundary layer thickness for the same Re_x). Since the Coriolis force increases linearly with the rate of rotation Ω, there is a linear relation between the boundary layer thickness and Ro_x/Re_x; this result agrees with the measurements of the two dimensional developing boundary layer in a rotating channel flow given by Koyama et al[2].

Because the normal component of the Coriolis force is much larger than the streamwise component of the force when Ro_x/Re_x is small, the calculated profile

appears to show some self-similarity. Figure 2.3 displays the velocity profile at two streamwise locations for $Ro_x/Re_x = 2x10^{-6}$ and $Ro_x/Re_x = 25x10^{-5}$ which correspond to low and high rotation rates respectively. The data points for the two downstream locations for $Ro_x/Re_x=2x10^{-6}$ are almost on top of one another. The profile is not exactly self-similar for fixed Ro_x/Re_x because of the streamwise component of the Coriolis force which causes a streamwise pressure gradient. At low Ro_x/Re_x, where the normal component dominates, the effect of the streamwise pressure gradient is below the resolution of observation. However, at sufficiently high Ro_x/Re_x, the effect of the streamwise pressure gradient and the absence of self-similarity become apparent. For example, a small amount of nonself-similarity can be seen in the data for $Ro_x/Re_x = 25x10^{-5}$ in Figure 2.3. If the profile was exactly self-similar, no such difference would exist. In addition, the bulge near the top of the boundary layer for $Ro_x/Re_x = 25x10^{-5}$ is reminiscent of boundary layer profiles with a favourable pressure gradient. This provides further evidence that the streamwise component of the Coriolis force has become significant.

2.4 Linear Stability of the Base Flow

Once the two dimensional base flow has been obtained, it is possible to study the linear stability of spanwise perturbations to this flow. Since the base flow is two dimensional, the study of spanwise perturbations to the flow is a three dimensional problem.

A typical plot of the growth rate of disturbances as a function of wavelength and Re_x is shown in Figure 2.4. The wavelength λ has been nondimensionalized as

$$\Lambda_{Re} = \frac{U_\infty \lambda}{\nu} \tag{8}$$

The most unstable wavelength is indicated by the dotted line. At a point sufficiently far downstream, the most unstable wavelength reaches an asymptotic value. This occurs once the wavelength of the vortices is small compared to the boundary layer thickness. From this point on, the flow viewed by the vortices is parallel and unchanging, as is the case for the Görtler problem[5,8].

The base flow used in most studies of the Görtler problem is the Blasius profile due to large radii of curvature. As shown earlier, the influence of the normal component of the Coriolis force suppresses the development of the rotating boundary layer and the profile is not Blasius. However, for a sufficiently low rotation rate, there is a negligible amount of error introduced by assuming a Blasius profile. It was found that rotation rates Ro_x/Re_x of the order 10^{-5} have about 5% error in the asymptotic wavelength using the Blasius solution as the base flow rather than the calculated profile. Consequently, for the purposes of this study, rotation rates Ro_x/Re_x below 10^{-5} will be described as "low rotation" and the Blasius solution is used as the base flow. For rotation rates above this value, termed "moderate" or "high rotation", the base flow has been calculated.

Figure 2.5 shows a comparison between experimentally measured wavelengths[4] and the calculated asymptotic wavelengths. As can be seen, the experimental wavelengths are generally larger than the most unstable wavelengths. This could be due to experimental conditions which cause larger wavelength vortices to be preferentially excited or which initially have more energy in long wavelength disturbances. For example, Guo & Finlay[5] showed that a misalignment between the leading edge of the plate and the flow of only half a degree caused the selection of wavelengths considerably greater than the most unstable wavelength for the Görtler problem. Figure 2.4 shows that the contours of growth rate are broader above the most unstable wavelength than below. Thus, given equal initial energy levels, it is more likely that wavelengths greater than the most unstable wavelength will be selected rather than wavelengths less than the most unstable. Floryan & Saric[9] showed that in an experiment, once the wavelength of Görtler vortices is selected near the leading edge, the vortices proceed downstream with this selected wavelength independently of the local growth rates further downstream. Thus, the observed wavelengths of the vortices are not necessarily the most unstable at that streamwise location.

2.4.1 Linear Stability for Low Rotation Rates

Matsubara and Masuda[4] demonstrated that for local linear stability, one of the parameters which governs the instability of a rotating boundary layer is

$$G_{rot}^2=\left(\frac{U_\infty\delta}{\nu}\right)^2\frac{\Omega\delta}{U_\infty}=Re_\delta^2 Ro_\delta \tag{9}$$

Note the similarity to the square of the Görtler number G used in the study of the concave boundary layer:

$$G=\frac{U_\infty\delta}{\nu}\left(\frac{\delta}{R}\right)^{1/2} \tag{10}$$

where the first portion describes the flow parameters and the second group describes the geometry of the system. Since the downstream location X has been used as the length scale in this study, G_{rot} can be written as:

$$G_{rot}=\left(\frac{U_\infty X}{\nu}\right)^{1/4}\left(\frac{\Omega X}{U_\infty}\right)^{1/2}=Re_x^{1/4}Ro_x^{1/2} \tag{11}$$

by using the relation between δ and x

$$\frac{\delta}{X}\propto\frac{1}{Re_x^{1/2}} \tag{12}$$

The rotational Görtler number can also be used to nondimensionalize the spanwise wavelength of the vortices λ

$$\Lambda_G=\frac{U_\infty\lambda}{\nu}\left(\frac{\Omega\lambda}{U_\infty}\right)^{1/2}=Re_\lambda Ro_\lambda^{1/2} \tag{13}$$

in the same manner as the Görtler problem. A plot of the growth rate of the vortices versus G_{rot} collapses to the same curve if Λ_G is the same. Therefore, for low rotation rates, the rotational Görtler number is sufficient to describe the

instability. Figure 2.6 shows the variation in the most unstable wavelength of the vortices as the rotational Görtler number is varied. Thus, the flow over a rotating flat plate shows a strong similarity to the Görtler problem at low rotation rates and it is appropriate to use the Blasius profile as the base flow.

2.4.2 Linear Stability for Moderate and High Rotation Rates

Once the rate of rotation has become sufficiently high that it is no longer appropriate to use the Blasius profile as the base flow, the rotational Görtler number is no longer suitable for describing the flow. It is not possible to combine the two parameters Ro_x and Re_x into a single variable that governs the growth of the vortices. Two cases having the same rotational Görtler number, but much different values of Ro_x and Re_x, have different values of the most unstable wavelength. This is due to the fact that the streamwise component of the Coriolis force has become sufficiently large to introduce a significant streamwise pressure gradient which eliminates the appearance of self-similarity of the velocity profile.

Figure 2.7 shows the variation in the most unstable wavelength as a function of Ro_x and Re_x. Because the Görtler number no longer applies, the other nondimensional wavelength defined earlier, Λ_{Re}, is used. This plot clearly illustrates the trends observed by Masuda & Matsubara[3] and Matsubara & Masuda[4]: the nondimensional spanwise spacing of the vortices decreases with increasing rotation and decreasing Reynolds number.

The earlier use of the variable Ro_x/Re_x in this study is also supported by this

data since the contours of dominant wavelength closely follow lines of constant Ro_x/Re_x below $Ro_x/Re_x = 10^{-5}$. However, for moderate and high rotation ($Ro_x/Re_x > 10^{-5}$), this is no longer the case and the most unstable wavelength is a function of both variables.

2.4.3 Comparison to Local Stability Analysis

The comparison of the results of local stability analysis and marching schemes for the Görtler problem has been the subject of much debate. Hall[5] (cf. also Day, Herbert & Saric[10]) showed that a marching technique does not produce unique neutral stability curves for the Görtler problem. In a local analysis, the partial differential equations that govern the stability of the flow are reduced to ordinary differential equations by neglecting some terms. Near the leading edge, ordinary differential equations are not a sufficient approximation of the full partial differential equations to describe the decay of the vortices near the outside edge of the boundary layer[5]. When the full partial differential equations are solved, the early stages of growth are different for different perturbations and it is not possible to construct unique neutral stability curves.

Similarly, it was found that neutral stability curves do not exist in the rotating boundary layer: the early stages of growth of the vortices depends on both the shape and the location of the initial perturbation. However, a short distance from the leading edge, the growth of all of the perturbations converges to one curve. This trend agrees with the results of Hall[5] for the Görtler problem. Hall[5]

found that the growth rates of all perturbations eventually converge to the neutral curve obtained by a local analysis further downstream for the Görtler problem.

Far away from the leading edge, the boundary layer thickness is much greater than the size of the vortices. Therefore, the use of ordinary differential equations to approximate the full partial differential equations is reasonable: it has been shown for the Görtler problem that the local stability and marching schemes produce similar results away from the leading edge[10]. Figure 2.5 shows that the asymptotic wavelength calculated in this study and previous local analysis[4] are approximately the same; there is a difference of about 7%.

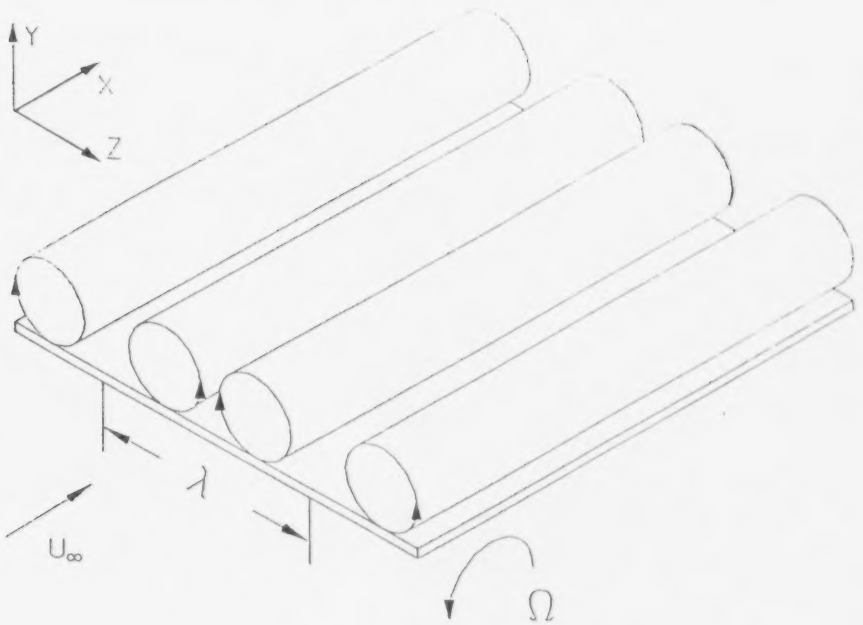

Figure 2.1. The geometry and sign convention of flow over a rotating flat plate is shown. Only a small section away from the leading edge is illustrated.

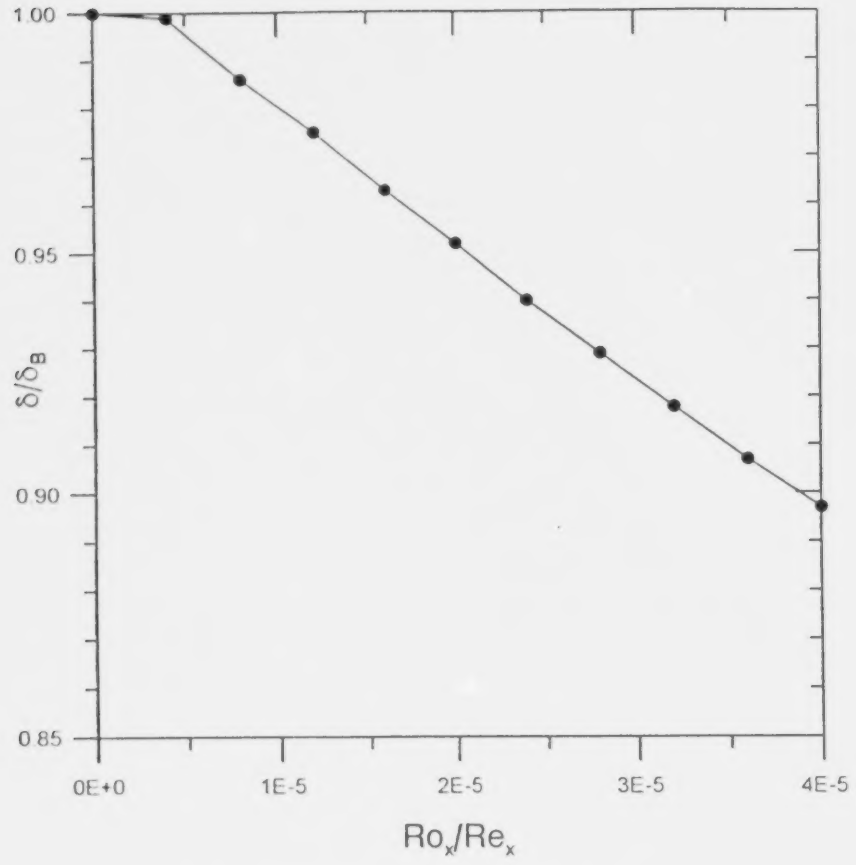

Figure 2.2. The variation in boundary layer thickness δ with rotation rate is compared to the nonrotating Blasius thickness δ_B.

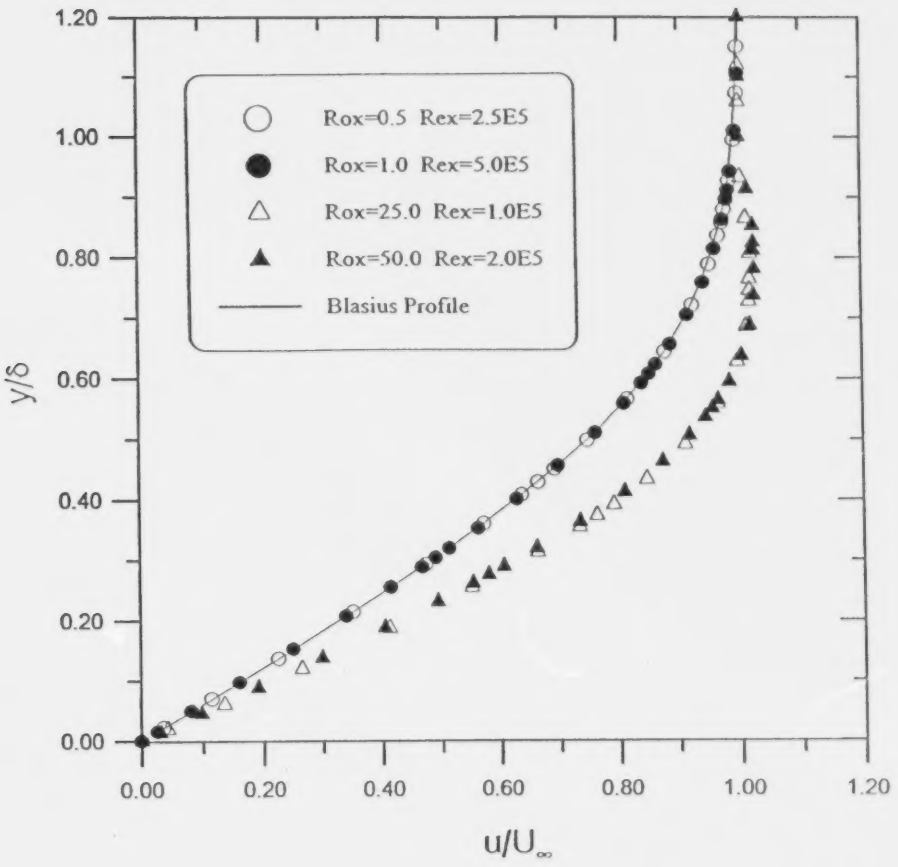

Figure 2.3. The velocity profile is shown for low rotation rate $Ro_x/Re_x = 2x10^{-6}$ (circles) and high rotation rate $Ro_x/Re_x = 25x10^{-5}$ (triangles).

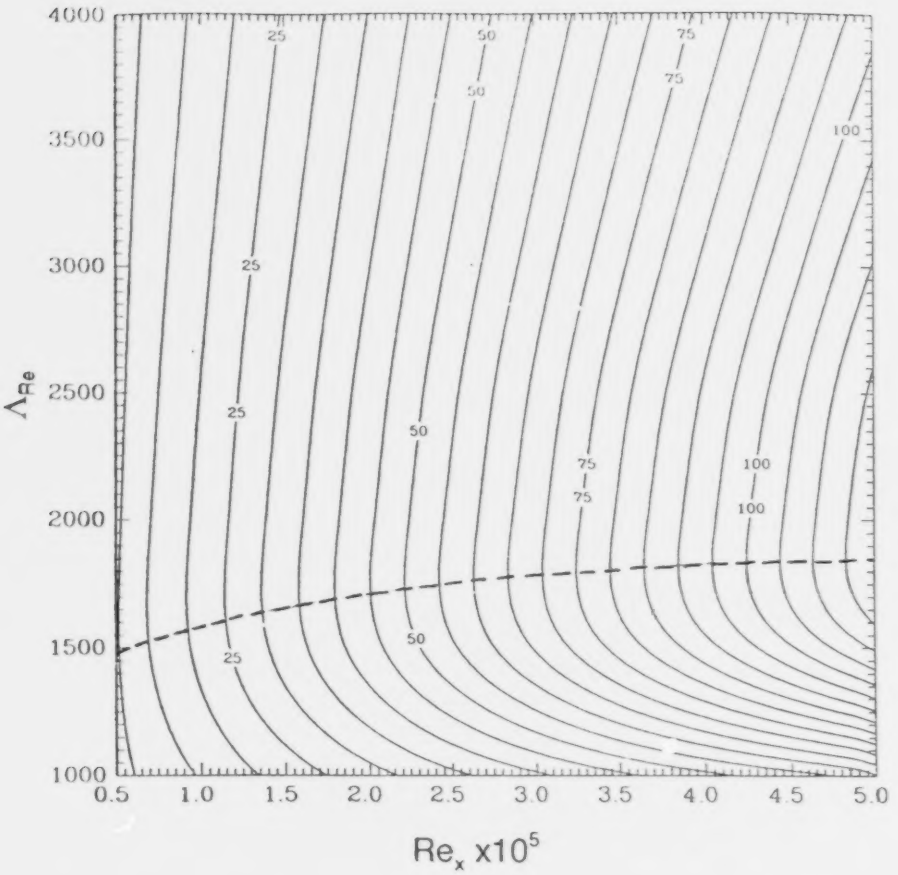

Figure 2.4. Variation in growth rate with Λ_{Re} and Re_x for $Ro_x/Re_x = 1x10^{-5}$. The most unstable wavelength is indicated by the dotted line.

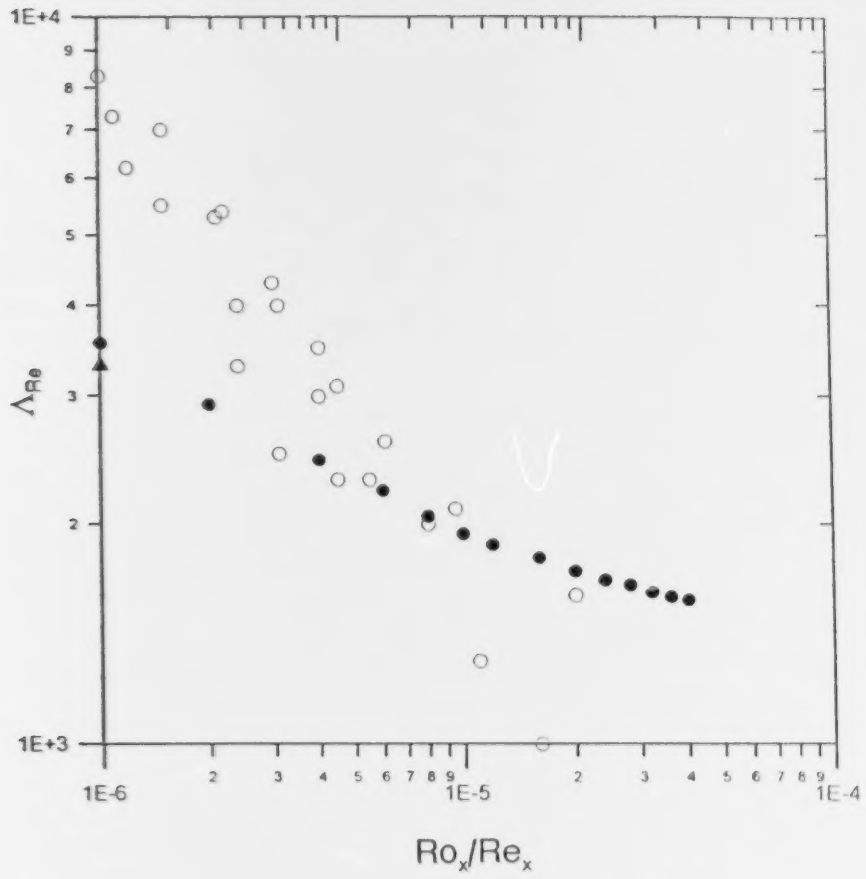

Figure 2.5. A comparison of experimentally observed wavelengths[4] (◯) and the linearly most unstable wavelengths calculated in this study (●) and a local stability analysis[4] (▲).

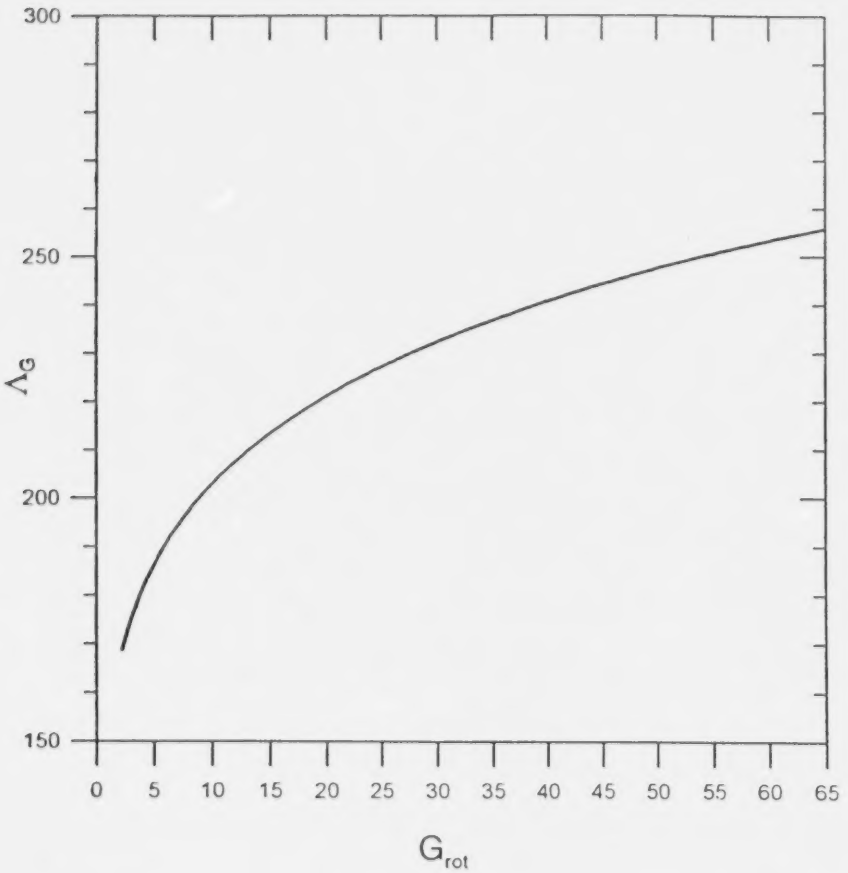

Figure 2.6. The variation in the linearly most unstable wavelength Λ_G of vortices with rotational Görtler number is shown. This figure is applicable to low rates of rotation ($Ro_x/Re_x \leq 10^{-5}$).

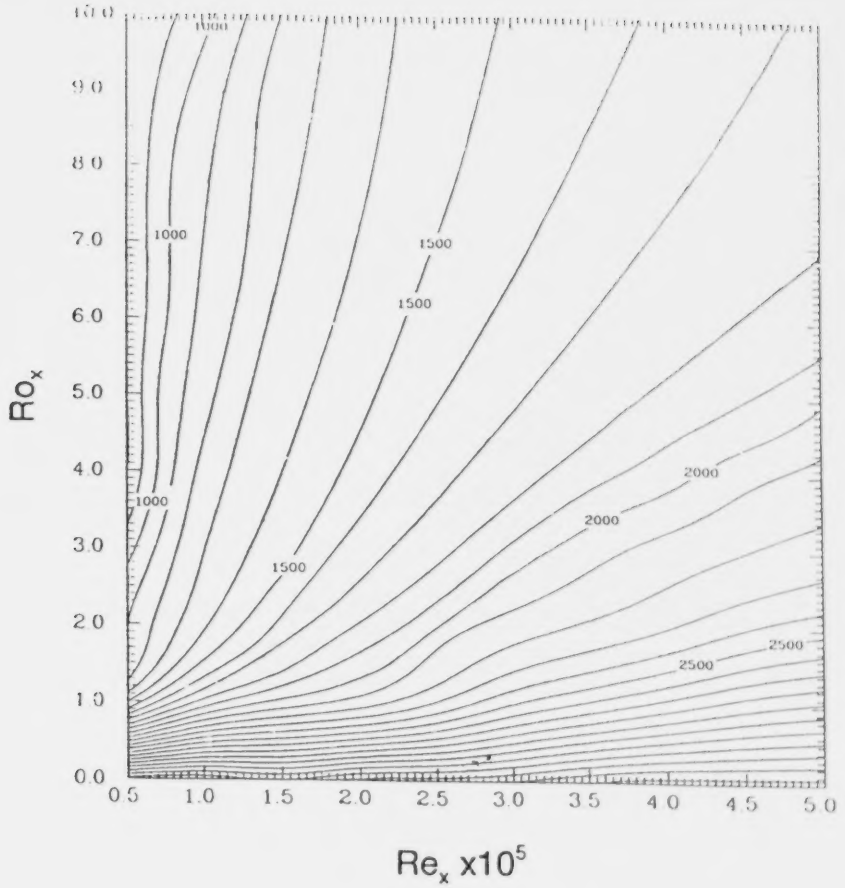

Figure 2.7. The linearly most unstable wavelength Λ_{Re} is shown as a function of Ro_x and Re_x.

CHAPTER 2 REFERENCES

[1] M. Chawla, "The stability of boundary layer flow subject to rotation", Ph. D. Thesis, Michigan State University (1969).

[2] H. Koyama, S. Masuda, I. Ariga, and I. Wantanabe, "Stabilizing and destabilizing effects of Coriolis force on two-dimensional laminar and turbulent boundary layers", Transactions of the ASME, **101,** 23 (1979).

[3] S. Masuda and M. Matsubara, "Visual study of boundary layer transition on rotating flat plate", Proc. 3rd IUTAM Symposium on Laminar-Turbulent Transition (1989).

[4] M. Matsubara and S. Masuda, "Three-dimensional instability in rotating boundary layer", Boundary Layer Stability and Transition to Turbulence ASME, **114**, 103 (1991).

[5] P. Hall, "The linear development of Gõrtler vortices in growing boundary layers", J. Fluid Mech., **130**, 41 (1983).

[6] Y. Guo and W.H. Finlay, "Wavenumber selection and irregularity of spatially developing nonlinear Dean and Gõrtler vortices", submitted to J. Fluid Mech.

[7] Y. Guo, "Secondary Instability of Dean and Gõrtler flow", Ph. D. Thesis, University of Alberta (1992).

[8] P. Hall, "Taylor-Görtler vortices in fully developed or boundary layer flows: linear theory", J. Fluid Mech., **124**, 475 (1982).

[9] J. Floryan and W. Saric, "Wavelength selection and growth of Görtler vortices", AIAA Journal, **22**, 1529 (1984).

[10] H.P. Day, T. Herbert, and W.S. Saric, "Comparing local and marching analyses of Görtler instability", AIAA Journal, **28**, 1010 (1990).

CHAPTER 3

3.0 CONCLUSION

3.1 Summary

In this analysis of the stability of flow over a rotating flat plate, it has been shown that the rotation suppresses the development of the boundary layer. As the amount of rotation is increased, the boundary layer thickness decreases. For rotation rates Ro_x/Re_x below 10^{-5}, the effect of rotation on the boundary layer development is minor and the Blasius profile can be used as the base flow. As the rotation rate increases above this value, the base flow begins to differ from the Blasius profile and the flow begins to lose its self-similarity. However, because the normal component of the Coriolis force is dominant for small Ro_x/Re_x, the flow is nearly self-similar. This is not exact self-similarity since there is a streamwise component of the Coriolis force that depends on streamwise location in a nonsimilar way. Once the rate of rotation is sufficiently high, this component of the Coriolis force causes a significant streamwise pressure gradient and the appearance of self-similarity is lost completely.

For low rotation rates (i.e. $Ro_x/Re_x < 10^{-5}$), the rotational Görtler number is the appropriate variable to describe the growth of the vortices. At higher rotation rates, the wavelength of the most unstable wavelength is a function of Ro_x

and Re_x and it is not possible to combine these variables into a single variable that governs the growth of the vortices. This is due to the loss of the self-similarity of the velocity profile.

A marching scheme was used to solve the governing equations. Like the Görtler problem, there is no unique neutral stability boundary for the rotating boundary layer. Far from the leading edge, local theory and the marching scheme give similar results.

3.2 Future Work

This study has considered only the linear growth of the vortices; the energy level of the vortices is infinitesimal. However, as the vortices continue to grow downstream, they begin to grow in a nonlinear fashion and a secondary stability mechanism becomes important. In general, a spanwise secondary instability may cause the vortices to interfere with each other. A vortex may split into a new pair if the vortices are far apart or two vortices may merge to form a single vortex if they are close together.

It has been shown that vortex splitting and merging occur for Dean vortices (vortices formed in a curved channel)[1]. However, in the Görtler problem, vortex splitting and merging events do not generally occur because the vortices have a smaller growth rate of secondary instability than Dean vortices[1]. Thus, the vortices may break down before a split or merge can occur. Instead, the vortices tend to distort when subjected to a spanwise perturbation[1]. One possible reason

for this difference may be related to the fact that Dean vortices occur in the presence of a streamwise pressure gradient while Görtler vortices do not.

If this is the case, the vortices in a rotating boundary layer may show two regimes of nonlinear behaviour. At low rotation rates when there is a strong analogy to the Görtler problem, the vortices may distort without significant splitting or merging. At high rotation rates, the streamwise component of the Coriolis force introduces a significant pressure gradient. Consequently, the splitting and merging events that characterize the nonlinear growth of Dean vortices may be observed.

CHAPTER 3 REFERENCES

[1] Y. Guo and W.H. Finlay, "Wavenumber selection and irregularity of spatially developing nonlinear Dean and Görtler vortices", submitted to J. Fluid Mech.

APPENDIX

Description of the Numerical Method

The parabolized Navier-Stokes equations are solved using the Legendre Spectral Element Method in a marching scheme. By incorporating the continuity equation, the general form of these equations can be written as:

$$2u_x\frac{\partial u_x}{\partial x}+\frac{\partial}{\partial y}(u_xu_y)+\frac{\partial}{\partial z}(u_xu_z)-f_x=-\frac{\partial p^*}{\partial x}+\frac{1}{Re_x}\left(\frac{\partial^2 u_x}{\partial y^2}+\frac{\partial^2 u_x}{\partial z^2}\right) \qquad \text{(A1)}$$

$$\frac{\partial}{\partial x}(u_xu_y)+\frac{\partial}{\partial y}(u_yu_y)+\frac{\partial}{\partial z}(u_yu_z)-f_y=-\frac{\partial p^*}{\partial y}+\frac{1}{Re_x}\left(\frac{\partial^2 u_y}{\partial y^2}+\frac{\partial^2 u_y}{\partial z^2}\right) \qquad \text{(A2)}$$

$$\frac{\partial}{\partial x}(u_xu_z)+\frac{\partial}{\partial y}(u_zu_y)+\frac{\partial}{\partial z}(u_zu_z)-f_z=-\frac{\partial p^*}{\partial z}+\frac{1}{Re_x}\left(\frac{\partial^2 u_z}{\partial y^2}+\frac{\partial^2 u_z}{\partial z^2}\right) \qquad \text{(A3)}$$

where **f** is a body force. For the rotating flat plate, f is the Coriolis force term and p^* is the sum of the pressure gradient and the centrifugal force (see equations (1), (2) and (6) in the main text). At a given location, the solution is marched downstream one step and the streamwise velocity is calculated at the new streamwise location using the x-momentum equation. A third order Adam-Bashforth scheme is used to march the nonlinear convection and force terms and a backward Euler scheme is used to march the linear terms. The pressure and the other components of velocity are determined at the new streamwise location from the other two components of the momentum equations and the continuity equation.

using a global iterative Uzawa scheme. Thus, the resulting matrix system can be written as:

$$2B_x^n \frac{U_x^{n+1}-U_x^n}{\Delta x}+\sum_{l=0}^{2}\beta_l(C_x-F_x)^{n-l}=-BP_x^{n+1}-\frac{1}{Re_x}AU_x^{n+1} \tag{A4}$$

in the streamwise direction and

$$\frac{B_x^{n+1}U_y^{n+1}-B_x^nU_y^n}{\Delta x}+\sum_{l=0}^{2}\beta_l(C_y-F_y)^{n-l}=-D_yP^{n+1}-\frac{1}{Re_x}AU_y^{n+1} \tag{A5}$$

$$\frac{B_x^{n+1}U_z^{n+1}-B_x^nU_z^n}{\Delta x}+\sum_{l=0}^{2}\beta_l(C_z-F_z)^{n-l}=-D_zP^{n+1}-\frac{1}{Re_x}AU_z^{n+1} \tag{A6}$$

in the cross stream plane. The continuity equation becomes

$$-D_y^TU_y^{n+1}-D_z^TU_z^{n+1}=\frac{B_p^T}{\Delta x}(U_x^{n+1}-U_x^n) \tag{A7}$$

The symbol U_i^n is the velocity vector at the Gauss-Lobatto/Gauss-Lobatto nodes at step n. The symbols A, B, and D are the standard Laplace matrix, the lumped mass matrix, and the gradient matrices respectively. C_i and F_i are the convection and force terms and β_l = 23/12, -16/12, and 5/12 for l = 0, 1, and 2.

The stability equations are produced by inserting

$$u=u^0+u'$$

into the parabolized Navier-Stokes equation. The base flow is $\mathbf{u}^0$ and $\mathbf{u}'$ is a spanwise perturbation of the form

$$u' = \tilde{u} \exp(i\beta z) \tag{A8}$$

Here β is the perturbation wavenumber and $\tilde{\mathbf{u}}$ is a complex eigenfunction.

Assuming that the perturbation also has slow streamwise variation, the terms with second derivatives in the x direction can be neglected. This results in the following parabolized equations

$$2\frac{\partial}{\partial x}(u_x^0 \tilde{u}_x) + w_x = \frac{1}{Re_x}\left(\frac{\partial \tilde{u}_x}{\partial y} + \frac{\partial \tilde{u}_x}{\partial z}\right) \tag{A9}$$

in the streamwise direction and

$$\frac{\partial}{\partial x}(u_x^0 \tilde{u}_y) + \frac{\partial}{\partial x}(u_y^0 \tilde{u}_x) + w_y = -\frac{\partial p}{\partial y} + \frac{1}{Re_x}\left(\frac{\partial \tilde{u}_y}{\partial y} + \frac{\partial \tilde{u}_y}{\partial z}\right) \tag{A10}$$

$$\frac{\partial}{\partial x}(u_x^0 \tilde{u}_z) + \frac{\partial}{\partial x}(u_z^0 \tilde{u}_x) + w_z = -\frac{\partial p}{\partial z} - i\beta p + \frac{1}{Re_x}\left(\frac{\partial \tilde{u}_z}{\partial y} + \frac{\partial \tilde{u}_z}{\partial z}\right) \tag{A11}$$

in the cross stream plane. The continuity equation is

$$-\frac{\partial \tilde{u}_y}{\partial y} - \left(\frac{\partial}{\partial z} + i\beta\right)\tilde{u}_z = \frac{\partial \tilde{u}_x}{\partial x} \tag{A12}$$

where

$$w_i = \frac{\partial}{\partial y}(u_y^0 \tilde{u}_i + \tilde{u}_y u_i^0) + \left(\frac{\partial}{\partial z} + i\beta\right)(u_z^0 \tilde{u}_i + \tilde{u}_z u_i^0) - \frac{1}{Re_x}\left(2i\beta \frac{\partial \tilde{u}_i}{\partial z} - \beta^2 \tilde{u}_i\right)$$

and i = x, y , and z.

The complex eigenfunction $\tilde{\mathbf{u}}$ at each streamwise location is determined

from the unique eigenvalues $\mathbf{u}^0$, Ro_x, Re_x and the spanwise wavenumber ß. Subsequently, the kinetic energy E_k of the perturbation at each streamwise location is obtained according to

$$E_k = \int |u'|^2 \, dy \, dz \tag{A13}$$

The nondimensional growth rate σ is then calculated from

$$\sigma = (\ln E_k^{n+1} - \ln E_k^n) \frac{l}{\Delta x} \tag{A14}$$

since

$$E_k = e^{\sigma x} \tag{A15}$$

for linear perturbations. Here l is the downstream distance used to nondimensionalize σ. Thus, one can calculate how the growth rate varies as the spanwise wavenumber of the perturbation ß is varied. To generate the data for the contour plots shown in the main text, several runs for the same Ro_x and Re_x are made with different ß. The most unstable wavelength is then obtained from the contour plots.